A model of near-sea ice phytoplankton blooms

C. W. Lester,[1,*] T. J. W. Wagner,[2] and Dylan E. McNamara[3]

[1] *Earth and Climate Sciences, Duke University*
[2] *Atmospheric and Oceanic Sciences, University of Wisconsin Madison*
[3] *Physics and Physical Oceanography, University of North Carolina Wilmington*

Author Contributions: All authors conceived of the study idea and developed the methodology. CWL carried out the analysis and wrote the first draft with input from TJWW. All authors contributed to revisions and the final manuscript.

SCIENTIFIC SIGNIFICANCE STATEMENT

Arctic spring blooms of phytoplankton mark the annual emergence of the region's ecosystem from winter dormancy. Satellite observations show that these blooms have increased in size and magnitude in recent years. Although this is expected with generally warmer conditions, it has been found that near-ice blooms are spatially correlated with cold and fresh surface water signatures from sea ice melt. This study develops an idealized model that describes how the environmental impact of meltwater influences the spread of phytoplankton spring blooms in the region. The results support the idea that melt-induced stratification of the surface ocean is an important driver of recent observed changes in near-ice bloom characteristics in the Arctic. This furthermore implies that future changes in sea ice cover under continued Arctic warming will have far-reaching consequences for the timing and spread of such blooms.

DATA AVAILABILITY STATEMENT

Observational data and metadata is available on Dryad at
`https://datadryad.org/stash/share/Wbkk_7jFkKctpOxFtuXpJEv2UEblAJ4O09wf0Jo_va8`.
Model code is available at
`https://github.com/connerlester/A-model-of-near-sea-ice-phytoplankton-blooms`.

ABSTRACT

Arctic phytoplankton spring blooms have increased in magnitude and extent over the past two decades, particularly in waters near the sea ice edge. We develop an idealized model of phytoplankton dynamics that takes into account the role of sea ice meltwater flux and its impact on surface mixed layer depth. Satellite observations feature a characteristic peak in phytoplankton concentration at around 100 km from the ice edge. Model dynamics capture this peak and overall structure of the phytoplankton distribution. In the model, the characteristic spatial scale emerges from a balance of exponential growth near the ice edge, horizontal advection, and increased decay with distance from the ice as the mixed layer deepens. Observations and data further agree in that meltwater impacts phytoplankton concentrations up to 1000 km from the ice edge. Results suggest that reduced meltwater input under future sea ice retreat may suppress spring phytoplankton blooms in the region.

Keywords: Phytoplankton Blooms, Sea Ice Edge, Arctic Ocean

* Corresponding author contact: conner.lester@duke.edu

I. INTRODUCTION

Phytoplankton blooms occur near the ocean surface along many coastlines around the world. These blooms fuel local ecosystems and provide sinks for atmospheric carbon (Behrenfeld and Boss 2014; Leu *et al.* 2015; Wassmann and Reigstad 2011). It is less typical for such blooms to be found far from land in open ocean environments. Exceptions to this are observed in the Arctic and Southern Oceans where two distinct types of blooms are commonplace: (i) under-ice blooms which are believed to contribute significantly to Arctic production but are difficult to quantify with satellite data (see, e.g., Arrigo *et al.* 2012, 2014; Clement Kinney *et al.* 2023, 2020) and (ii) large open-ocean blooms near the edges of sea ice (Arrigo and Van Dijken 2003; Behrenfeld *et al.* 2017; Matrai *et al.* 2013; Moreau *et al.* 2019; Zhao *et al.* 2022), which are the focus of this study. We note that the link between under-ice blooms and near-ice open-ocean blooms remains a topic of ongoing research (e.g., Ardyna *et al.* 2020). A region with prominent near-ice blooms are the open waters between Greenland and the Svalbard Archipelago, encompassing Fram Strait and parts of the Greenland and Norwegian Seas (henceforth referred to simply as Fram Strait, see Figure 1). This region experiences annual spring bursts of large phytoplankton populations near the sea ice edge (Cherkasheva *et al.* 2014; Mayot *et al.* 2020). One remarkable feature of these ice-edge blooms is they are spatially correlated with relatively cold and fresh sea ice meltwater, which is suggested to be a key driver in bloom development (Castagno *et al.* 2023; Lester *et al.* 2021; Mayot *et al.* 2020). Over the past two decades, Fram Strait has seen an increase in phytoplankton bloom intensities (Lewis *et al.* 2020; Nöthig *et al.* 2015), and these changes have been linked to increased freshwater flux from sea ice melt (Castagno *et al.* 2023).

Here, we focus on the biophysical dynamics of springtime phytoplankton blooms in open water near the sea ice edge. We expand on the idealized model of ice-edge blooms of Lester *et al.* (2021). This previous work describes a characteristic "bloom curve", which represents the distribution of phytoplankton with distance from the sea ice edge as a function of meltwater input. Here, we show that this curve is consistent with the long-term mean distribution of near-surface chlorophyll *a* (chl-a) in Fram Strait, as observed from a decade of ocean color satellite retrievals. We refine the original model by representing changes in mixed layer depth, and constrain model parameters using satellite observations of chl-a, sea surface salinity (SSS), and sea ice concentration (SIC). We argue that a key control on spring blooms—surface stratification and associated mixed layer depth—is linked to SSS perturbations from sea ice meltwater near the ice edge. Our results suggest that ice-edge phytoplankton bloom dynamics can be described, to leading order, by (i) exponential growth at the ice edge via photosynthesis in a shallow mixed layer that is stratified by sea ice meltwater and (ii) decay of the bloom signal as vertical mixing causes the surface mixed layer to deepen which reduces exposure to sunlight and thereby growth. This simplified picture of complex ice-edge bloom dynamics builds understanding of how annual ice-edge blooms may evolve with climate change and particularly under continued sea ice retreat. Notably, this perspective also suggests the cessation of large open ocean blooms in the region if/when Fram Strait becomes sea ice-free.

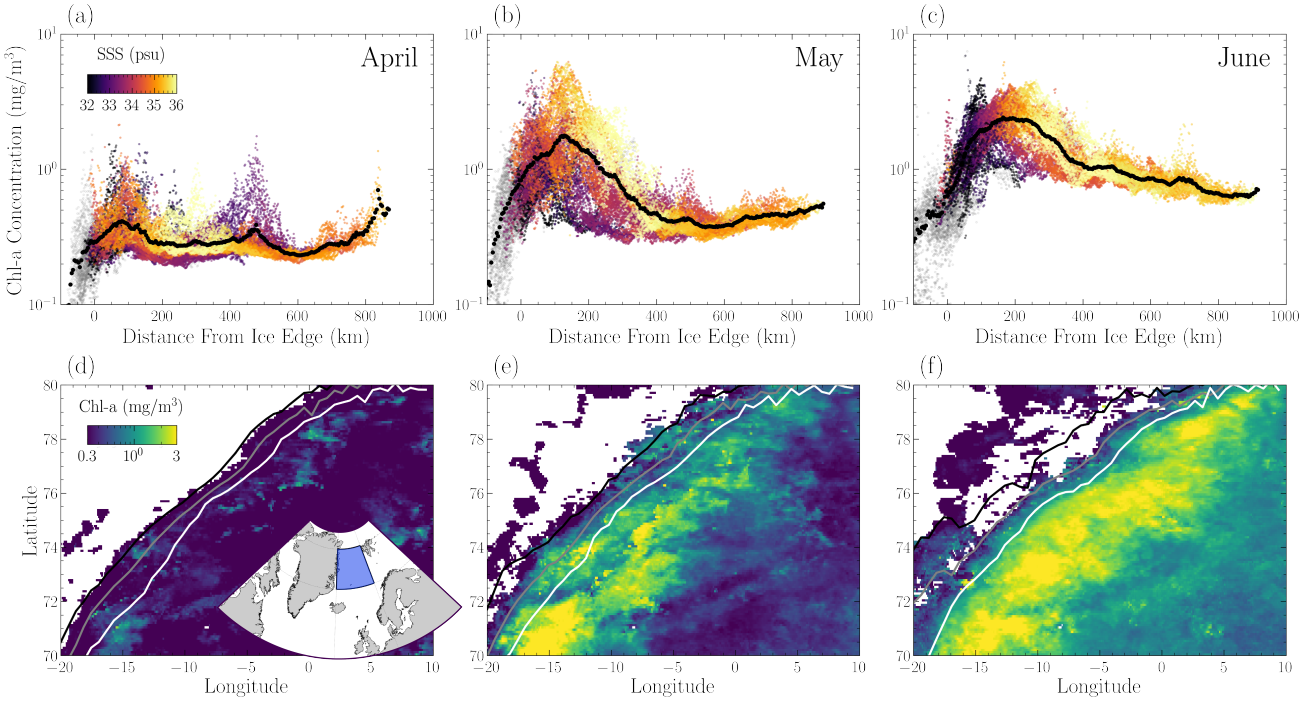

FIG. 1. Chl-a concentrations for April, May, and June, averaged over the years 2011–2019. Concentrations are data composites from MODIS Aqua and Terra and VIIRS-SNPP (NASA Ocean Biology Processing Group, GSFC 2017, 2021, 2022, see SI Section S5 for details). The study region is shown in blue in the map inset of panel (d). Top row panels (a,b,c) show log-scale chl-a vs distance from sea ice edge where data points are raw data from maps (d,e,f), respectively, and are colored by associated SSS values (see Figure 2). Grey points are chl-a values without an associated SSS value. Black points are binned averages. Bottom row panels (d,e,f) show chl-a concentration maps of Fram Strait. White regions indicate missing chl-a data due to presence of sea ice. Lines show the average ice-edge location at 75% (black), 50% (grey) and 15% (white) sea ice concentration for each month from the NASA Team algorithm (Cavalieri *et al.* 1996). For panels (a,b,c) we use sea ice concentration of 50% to define the ice edge $x = 0$. The occurrence of non-zero chl-a values inside the longterm mean sea-ice edge is the result of retaining chl-a observations in individual scenes where the ice edge is further retreated than its mean state.

II. AN IDEALIZED MODEL OF NEAR-ICE BLOOM DYNAMICS

The dynamics of phytoplankton blooms near the sea ice edge are highly complex and governed by numerous factors, including water temperature, sunlight intensity, nutrient type and availability, fluid stratification and transport, predation, and more (e.g., Behrenfeld and Boss 2014). Our aim is to gain understanding of specific key processes by applying several simplifying assumptions, thereby reducing the complexity of the system and making it conceptually and mathematically tractable.

We consider the near-surface phytoplankton concentration $P(\boldsymbol{x}, t)$, averaged over the mixed layer depth, $D(\boldsymbol{x}, t)$, with coordinates $\boldsymbol{x} = (x, y)$ where x is perpendicular and y is parallel to the ice-edge (see Supplementary Information, SI, for details). We assume that P evolves to leading order with gains from sunlight-dependent growth and losses from mortality and sinking. Phytoplankton are treated as passively moving biological tracers. Within the mixed layer D we assume that P, as well as other tracers such as temperature and salinity are well mixed and approximately homogeneous. Below the mixed layer, phytoplankton concentration decreases rapidly and we take $P \to 0$ for depths greater than D. We express the evolution of $P(\boldsymbol{x}, t)$ through mass conservation as

$$\partial_t P + \boldsymbol{u} \cdot \boldsymbol{\nabla} P = \Gamma(P, D)P, \tag{1}$$

where ∂_t is the first time derivative, $\boldsymbol{u}(\boldsymbol{x}, t)$ is the turbulent horizontal velocity field and Γ is the depth averaged net growth rate that decreases with increasing P and D—and thus varies spatially with distance from the ice edge. We note that this representation of spatially variable phytoplankton growth $\Gamma(P(\boldsymbol{x}), D(\boldsymbol{x}))$ in a turbulent flow field is a generalization of the work by Birch *et al.* (2007), who computed bounds on biomass and productivity for specific growth and decay scalings.

A major control on phytoplankton growth is the availability of sunlight, and phytoplankton blooms are initiated in early spring as the Arctic emerges from dark, sunless winter. As phytoplankton are mixed around in the water column they experience a range of light conditions at different depths and times of day. Toward the bottom of the mixed layer they are exposed to little sunlight and grow relatively slowly, compared to the surface. For low enough light intensity or deep enough mixed layer depths, phytoplankton grow in proportion to the available sunlight—also known as "light-limited" growth. And even for higher surface light intensities, phytoplankton growth in the starkly fluctuating light environment of the mixed layer tends towards the light-limited regime (Köhler *et al.* 2018), which we will apply to Γ in our model. This approximation is in part motivated by previous results in Richardson *et al.* (2005) that light availability is the dominant control for Greenland Sea spring primary production. Growth is reduced when biomass in the mixed layer increases sufficiently to cause the attenuation of light in the phytoplankton cloud, providing a self-regulating and stabilizing feedback (see SI Section S3) (Huisman 1999; Lorenzen 1972). We write the total net growth as

$$\Gamma(P, D) = \gamma I(P, D) - r - \frac{w_P}{D} - \frac{w(D)}{D}, \tag{2}$$

where γ is an effective growth rate determined by sunlight intensity at the surface and $I(P, D)$ is the depth averaged light intensity (normalized by the surface light intensity) which decreases with P and D, r is the effective mortality/community respiration rate, w_P is the sinking rate, and the final term is the dilution rate due to the rate of change of the mixed layer depth $w(D)$ (see cartoon in SI Figure S1).

Mesozooplankton predation is not explicitly represented in Equation (2). Grazing by mesozooplankton is highly variable and complex, and for simplicity we take predation to be small relative to the other decay terms during these spring blooms. Beside simplicity, our choice is motivated by the argument that most grazing in the region occurs after peak-bloom conditions (Norrbin *et al.* 2009) and that, for example, *Calanus glacialis* nauplii abundance reaches its maximum later in the season (Søreide *et al.* 2010). Furthermore, we assume that the growth rate Γ is not inhibited by nutrient limitations within the mixed layer for the early spring blooms that we are primarily interested in. This is in line with previous findings that nutrients in the region are not depleted until roughly July–August (Lewis *et al.* 2019; Richardson *et al.* 2005). We note that the omission of nutrient dynamics should be considered an important caveat for the later bloom stages and termination questions. Finally, a question for future consideration is how these

open-water blooms are influenced by preceding under-ice blooms, which may both deplete nutrients early or act in a seeding capacity for the later stages (e.g., Ardyna *et al.* 2020).

Sea ice meltwater stratifies the upper water column, effectively reducing the mixed layer depth and allowing phytoplankton to stay near the sunbathed surface and multiply. Sea ice meltwater is most concentrated at the ice edge (Castagno *et al.* 2023), and the surface is highly stratified with shallow mixed layer depth $D_0 = D(x = 0)$ (von Appen *et al.* 2021; Peralta-Ferriz and Woodgate 2015). Away from the ice edge the meltwater mixes with the saltier ambient ocean water and the stratification is weakened, leading to an increase in $D(\boldsymbol{x}, t)$. In the far-field open ocean the plankton concentration approaches a background steady state $P_\infty \sim 1/D_\infty$, set by the open ocean mixed layer depth D_∞ (SI Section S4)—a relationship predicted in previous models and seen in observations (Huisman 1999; Smith Jr and Jones 2015; Talling 1957). These dynamics for $P(\boldsymbol{x}, t)$ suggest that the observed surface plankton concentrations arise as a balance of rapid growth when low plankton concentrations are advected from the sea ice edge into open waters, and decay far from the ice edge from reduced light availability, death, sinking, and dilution as the mixed layer depth increases with the loss of meltwater stratification (Figure 1).

We apply a simplified treatment of the evolution of the mixed layer depth $D(\boldsymbol{x}, t)$ as a fluid boundary problem that can be described using the material derivative such that

$$\partial_t D + \boldsymbol{u} \cdot \boldsymbol{\nabla} D = w(D), \tag{3}$$

where $w(D)$ is the average rate of change of $D(\boldsymbol{x}, t)$. Equation (3) describes the rate at which the mixed layer depth evolves from D_0 at the ice edge towards D_∞ through weakening of meltwater stratification and vertical mixing.

As pointed out in Lester *et al.* (2021), on individual bloom time and spatial scales it is difficult to establish a characteristic spatial bloom curve for $P(\boldsymbol{x})$, due to high spatial heterogeneity in the presence of turbulent mixing, $\boldsymbol{u}(\boldsymbol{x}, t)$. However, when averaged over a sufficiently large set of blooms and seasons the heterogeneity is smoothed and clear spatial patterns emerge, as shown below.

For a given spring month we approximate the system averaged along the ice edge to be in quasi-steady state, varying slowly over the monthly time scale T_M (Figure 1)—much slower than bloom time scale $T_B \sim \gamma^{-1}$ of order days, such that $T_B \ll T_M$. We consider small fluctuations about the mean phytoplankton concentration $P(\boldsymbol{x}, t) = \overline{P}(x) + P'(\boldsymbol{x}, t)$, mixed layer depth $D(\boldsymbol{x}, t) = \overline{D}(x) + D'(\boldsymbol{x}, t)$ and horizontal flow $\boldsymbol{u}(\boldsymbol{x}, t) = \overline{\boldsymbol{U}} + \boldsymbol{u}'(\boldsymbol{x}, t)$ in Equations (1) and (3). Quantities $\overline{P}$, $\overline{D}$ and $\overline{\boldsymbol{U}}$ are averaged along the ice edge, y, and over a given month. To a first approximation, the average dynamics of Equations (1) and (3) reduce to

$$U \frac{\mathrm{d}\overline{P}}{\mathrm{d}x} \simeq \Gamma(\overline{P}, \overline{D})\overline{P} \quad \text{and} \quad U \frac{\mathrm{d}\overline{D}}{\mathrm{d}x} \simeq w(\overline{D}). \tag{4}$$

Here U is a representation of average advective flow normal to the ice edge. Note that the dominant near-surface current for much of the study region flows along the ice edge with the East Greenland current. However, since we are solely concerned with the across-ice edge perspective we disregard the along-ice edge flow component (SI Section

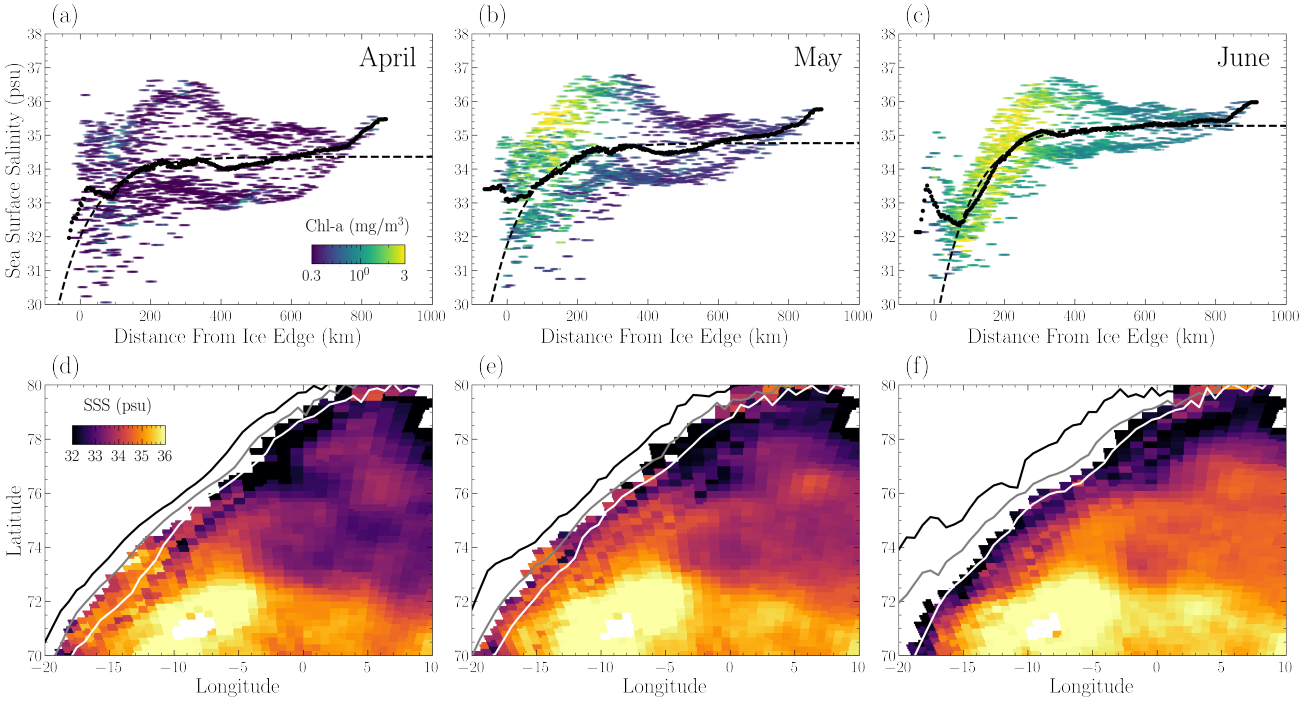

FIG. 2. Sea surface salinity (SSS) for April, May and June averaged over the years 2011-2019 (Supply *et al.* 2020, see SI Section S5). Top row panels (a,b,c) show SSS vs distance from sea ice edge where data points are raw data from maps (d,e,f), respectively, and are colored by associated chl-a values (see Figure 1). Solid black points are binned averages and dashed lines are fitted e-folding curves with saturation length scale $L_{\mathrm{SSS}} = 100$ km. Fits for L_{SSS} vary little between months and are thus held constant at 100 km for simplicity. Bottom row panels (d,e,f) show SSS maps of Fram Strait. As in Figure 1, white regions indicate missing data due to presence of sea ice and lines show the average ice-edge location at SIC = 75% (black), 50% (grey) and 15% (white). Again, panels (a,b,c) use SIC = 50% to define $x = 0$. We note that the concentrated region of high SSS $\gtrsim 35$ psu is around the island of Jan Mayen. Excluding data near Jan Mayen ($\sim 9°$W, 71°N) does not significantly change the results—it primarily reduces the average SSS(x) in panels (a,b,c) by a constant offset, and it does not notably alter the chl-a(x) distributions of Figure 1.

S2). The result of advection from U leads to transporting meltwater into the open ocean (e.g., Castagno *et al.* 2023; Lester *et al.* 2021). We note that model results are similar if we assume that turbulent diffusion dominates advection. From here on, we consider only the monthly-averaged fields, and will drop the overlines for clarity of presentation.

Near the ice edge, the mean phytoplankton concentration undergoes exponential growth as

$$P(x) \sim P_0 e^{x/L_P}, \tag{5}$$

where $L_P = U/\Gamma(P_0, D_0)$ is a characteristic length scale that balances the horizontal transport with the plankton growth rate. Far from the ice edge the concentration decays towards $P(x) \to P_\infty \sim 1/D_\infty$, suggesting that the surface phytoplankton concentration is maximized at some nontrivial distance away from the ice edge and thus defining the characteristic bloom curve $P(x)$.

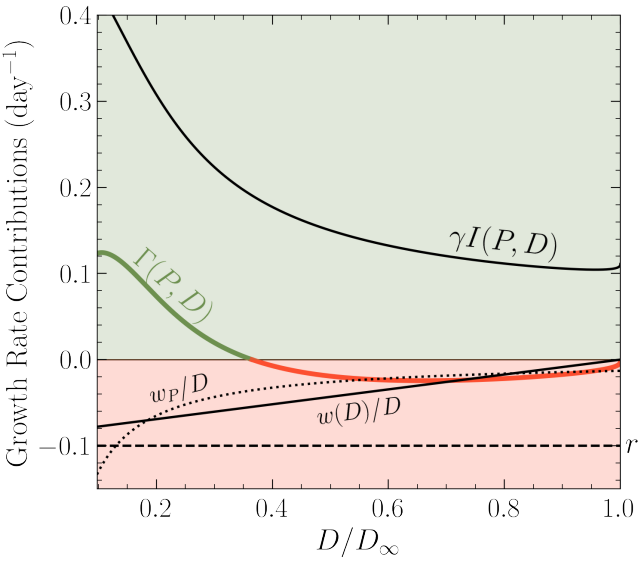

FIG. 3. Depth averaged net growth rate $\Gamma(P, D)$ partitioned by individual contributions as a function of rescaled mixed layer depth D/D_∞. Green region is positive growth and red is negative growth (phytoplankton death/loss and dilution of the average P). Parameters are as used for the month of June in Figure 4. Other months look similar.

III. RESULTS AND DISCUSSION

To observe the spatial patterns of ice-edge blooms we analyze monthly averages of surface chl-a concentrations in Fram Strait from 2011–2019 (see SI Section S5 for details). As seen in Figure 1 these monthly averages reveal patterns of steep chl-a increase near the ice edge and more gradual decay towards the open ocean, supporting the general bloom curve from Lester *et al.* (2021). We next consider whether the model of Equations (4) can capture this feature.

In order to constrain our model using observations, we use SSS as a proxy of mixed layer depth, motivated by the observed dominance of near-surface stratification in determining the variability of mixed layer depth (Peralta-Ferriz and Woodgate 2015). Recent advances in satellite techniques mean that SSS in the Arctic can be observed with good spatial and temporal cover, while direct measurements of mixed layer depths are much more sporadic. Figure 2 shows spatial patterns of SSS for spring months averaged over the study period (SI Section S5), exhibiting patterns of low SSS near the ice edge, suggesting a shallow mixed layer, and high SSS far from the ice edge, suggesting a larger mixed layer. When averaged along the sea ice edge the pattern is accentuated, revealing how surface salinity relaxes from $\mathrm{SSS}_0 \sim 30 - 33$ psu to $\mathrm{SSS}_\infty \sim 35$ psu at a rate determined by the saturation length scale L_{SSS} (Figure 2).

If D is primarily a function of SSS, then for small perturbations to SSS_∞ we can write $D_\infty - D \propto \mathrm{SSS}_\infty - \mathrm{SSS}$ and thus $\mathrm{d}D/\mathrm{d}x \propto \mathrm{dSSS}/\mathrm{d}x$. We therefore model the mixed layer gradient as

$$\frac{\mathrm{d}D}{\mathrm{d}x} \simeq \frac{D}{L_D}\left(1 - \frac{D}{D_\infty}\right), \tag{6}$$

where $L_D \simeq L_{\mathrm{SSS}}$. This representation of $D(x)$ allows for a closed solution to the average phytoplankton distribution

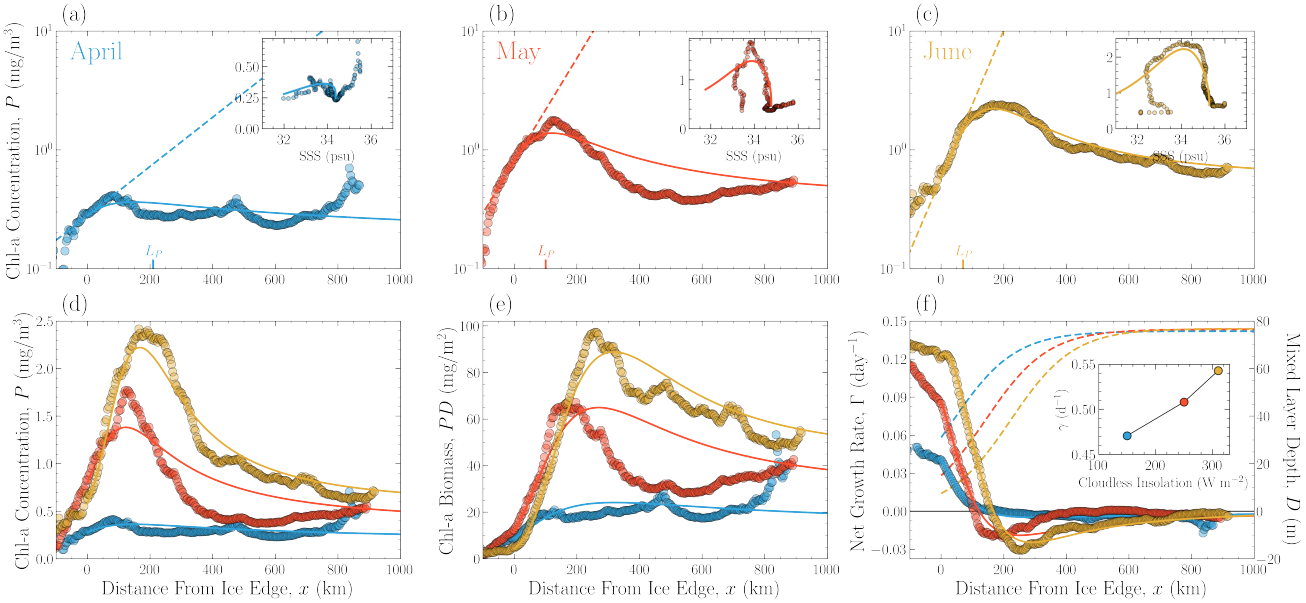

FIG. 4. Model-observation comparison for P and chl-a. Top row panels (a,b,c) show chl-a concentration vs distance from the mean ice edge. Markers correspond to the mean values (black dots) from Figure 1. Dashed lines are exponential growth functions (Eq. 5) giving the length scale $L_P = U/\Gamma(P_0, D_0)$—marked on the horizontal axis of each plot. Solid lines show solutions of $P(x)$ for Equations (4) and (6) using $L_D = 100$ km and fit parameter $D_0 = 31, 15, 7.5$ m for April, May, and June. Insets show binned chl-a concentrations vs binned SSS values from Figure 2 (markers). Lines are the $P(x)$ solutions of the larger panels vs the fitted SSS(x) from the dashed lines in Figure 2. Panel (d) overlays the information from panels (a,b,c) on a linear scale. Panel (e) shows integrated biomass $P(x)D(x)$ (lines) and chl-a$(x)D(x)$ (markers) using the modeled mixed layer depths $D(x)$. Panel (f) shows the dependence of growth rate $\Gamma(P, D)$ (Eq. 2) on distance from the ice edge. Markers are computed from Equation (2) using chl-a(x) distributions and model parameters from predictions in (a,b,c). The dashed lines in (f) show the modeled mixed layer depths $D(x)$ (right axis) and the inset shows an estimate of the growth rate scale γ (SI Eq. S2) plotted against observed clear-sky insolation in Fram Strait for each month (insolation data from Castagno *et al.* (2023)).

$P(x)$ which is a function of (i) parameters that are broadly independent of the particular bloom: γI, r, and w_P; (ii) bloom-specific and in principle measurable parameters such as phytoplankton concentrations at the ice edge P_0 and in the open ocean P_∞; (iii) the length scales L_P and L_D; and (iv) the mixed layer depths D_0 and D_∞. Observations of mean chl-a(x) in Figure 1 allow us to infer P_0 and P_∞ if we assume $P \propto$ chl-a. The growth length scale L_P can be estimated from the rate of exponential growth near the ice edge (Figures 1, 4). From observations of SSS(x) in Figure 2 we can approximate the length scale $L_D \simeq L_{\mathrm{SSS}}$.

Due to lack of in-situ measurements of surface insolation and the complexity of phytoplankton growth under fluctuating light conditions (Köhler *et al.* 2018) it is challenging to directly measure the light dependent growth rate scale γ. We similarly do not have direct measurements of D_0 or D_∞. However, we are able to estimate the value of γ from measurements of L_P and we can approximate the mixed layer depth D_∞ from the dynamics that lead to P_∞ (see SI Section S4 for details). Thus our model only uses a single unconstrained fitting parameter, D_0. For the three months under consideration here, we find best fits between the observed chl-a distribution and the theoretical bloom curves when $D_0 = 31$ m in April, $D_0 = 15$ m in May, and $D_0 = 7.5$ m in June. These values agree well with measurements in the region (Peralta-Ferriz and Woodgate 2015). The relative importance of the individual terms in Equation (2) for these parameter values is shown in Figure 3.

From the monthly values of chl-a(x) averaged over the years 2011–2019 (Figures 1, 4; SI Section S5) we are able to capture the start of the spring phytoplankton bloom season in Fram Strait, and also the spatial bloom curve as a function of distance to the ice edge for each month. Close to the sea ice edge we observe exponential growth trends as predicted above (Equation 5) with length scale L_P varying around ~ 100 km. The approximated growth rate γ is found to be around 0.5 day^{-1}—consistent with measurements (Eppley 1972; Huisman 1999; Smith Jr *et al.* 1987). Additionally, the estimated γ values increase with clear-sky insolation in Fram Strait from April to June (Figure 4f, inset), supporting our assumption that blooms are in a light-limited regime.

The observations are consistent with the dynamics proposed in this model: when phytoplankton are initially advected from the ice edge into open water, they grow quickly within a shallow mixed layer that is stratified by sea ice meltwater. As they are further advected and grow the meltwater begins to mix with the ocean waters. This elevates SSS and reduces the capacity of phytoplankton growth as the mixed layer deepens (Huisman 1999). In between the extremes of exponential phytoplankton growth at the ice edge, marked by low chl-a and low SSS, and bloom decay far from the ice edge, marked by low chl-a and high open-ocean SSS, we observe the chl-a maximum. This is located at an intermediate SSS value (~ 34 psu) at a characteristic distance (~ 100 km) from the ice edge (Figure 4).

The model predicts that the bloom magnitude $P_{\max} \sim \gamma/D_0 \sim \gamma M_0$ increases with the growth rate scale γ as well as the sea ice melt rate at the ice edge $M_0 \sim 1/D_0$ (see SI Section S4). This is noteworthy because both of these parameters are subject to vary under climate change: γ will likely increase with surface temperatures (Eppley 1972) and be impacted by changes in cloud cover, while the melt rate M_0 stands to increase as surface temperatures increase under global warming (at least transiently), exacerbated in this region by Arctic Amplification (England *et al.* 2021). This combination of factors suggests that in the near-term ice-edge phytoplankton blooms will continue to increase in magnitude and appear earlier in the spring. Importantly however, a retreat of sea ice in the region would signify reduced blooming. If Fram Strait becomes sea ice free in the spring months, the model implies the cessation of these characteristic bloom curves.

Lastly, we note an important consequence of considering the depth-averaged plankton concentration $P(x)$ as a property of the mixed layer depth: In this framework, the total biomass is given by $B(x) = P(x)D(x)$. The biomass distribution B is less strongly dependent on x than P is, since a part of the x-dependence is due to the compression/dilution that results from changes in D. As a result, $P_{\max} \simeq 4P_\infty$, while the peak in biomass $B_{\max}$ is only roughly twice that of B_∞ (Figure 4e). In other words, in this model approximately half of the near-surface plankton peak near the ice edge is due to increased growth and the other half is due to the plankton being confined more closely to the surface. This also suggests that at least part of the observed recent increases in near-surface chl-a in the Fram Strait region may be due to the plankton being more closely confined to the surface, rather than purely an increase in overall biomass.

IV. CONCLUSION

We have presented an idealized modeling framework to explore the influence of sea ice melt on the distribution of phytoplankton during the spring blooming period. By accounting for the impacts of light-limited growth, meltwater-induced stratification of the mixed layer, and advection away from the ice edge, the model reproduces observed characteristic spatial distributions. The model results support the idea that freshwater flux from sea ice melt plays a crucial role in determining the magnitude and spread of near-ice phytoplankton blooms. This is largely because increased surface stratification causes phytoplankton to spend more time exposed to sunlight, leading to faster growth. Our results motivate the need for measurements that can better elucidate the relationships between meltwater input, near-surface water column conditions, and plankton growth. This, together with continued modeling efforts will allow us to better constrain meltwater effects on the mixed layer depth and the resulting plankton concentration and biomass curves with distance from the ice edge. Irrespective of the details of these relationships, our findings support the broader notion that meltwater plays a key role in Arctic ecosystem dynamics. Continued rapid changes in sea ice cover and associated melt input can therefore be expected to fundamentally change the growth patterns of phytoplankton and thereby stand to impact the regional ecosystem as a whole.

von Appen, W.-J., A. M. Waite, M. Bergmann, C. Bienhold, O. Boebel, A. Bracher, B. Cisewski, J. Hagemann, M. Hoppema, M. H. Iversen, *et al.* (2021), Nature Communications **12** (1), 7309.

Ardyna, M., C. Mundy, N. Mayot, L. C. Matthes, L. Oziel, C. Horvat, E. Leu, P. Assmy, V. Hill, P. A. Matrai, *et al.* (2020), Frontiers in Marine Science **7**, 608032.

Arrigo, K. R., D. K. Perovich, R. S. Pickart, Z. W. Brown, G. L. Van Dijken, K. E. Lowry, M. M. Mills, M. A. Palmer, W. M. Balch, F. Bahr, *et al.* (2012), Science **336** (6087), 1408.

Arrigo, K. R., D. K. Perovich, R. S. Pickart, Z. W. Brown, G. L. Van Dijken, K. E. Lowry, M. M. Mills, M. A. Palmer, W. M. Balch, N. R. Bates, *et al.* (2014), Deep Sea Research Part II: Topical Studies in Oceanography **105**, 1.

Arrigo, K. R., and G. L. Van Dijken (2003), Journal of Geophysical Research: Oceans **108**, C8.

Behrenfeld, M. J., and E. S. Boss (2014), Annual Review of Marine Science **6** (1), 167.

Behrenfeld, M. J., Y. Hu, R. T. O'Malley, E. S. Boss, C. A. Hostetler, D. A. Siegel, J. L. Sarmiento, J. Schulien, J. W. Hair, X. Lu, *et al.* (2017), Nature Geoscience **10** (2), 118.

Birch, D. A., Y.-K. Tsang, and W. R. Young (2007), Physical Review E **75** (6), 066304.

Castagno, A. P., T. J. W. Wagner, M. R. Cape, C. W. Lester, E. Bailey, C. Alves-de Souza, R. A. York, and A. H. Fleming (2023), Global Change Biology **29** (17), 5087, https://onlinelibrary.wiley.com/doi/pdf/10.1111/gcb.16815.

Cavalieri, D. J., C. Parkinson, P. Gloersen, and H. J. Zwally (1996), "Sea ice concentrations from Nimbus-7 SMMR and DMSP SSM/I-SSMIS passive microwave data,".

Cherkasheva, A., A. Bracher, C. Melsheimer, C. Köberle, R. Gerdes, E.-M. Nöthig, E. Bauerfeind, and A. Boetius (2014), Journal of Marine Systems **132**, 196.

Clement Kinney, J., M. Frants, W. Maslowski, R. Osinski, N. Jeffery, M. Jin, and Y. J. Lee (2023), Journal of Geophysical Research: Oceans **128** (9), e2022JC019000.

Clement Kinney, J., W. Maslowski, R. Osinski, M. Jin, M. Frants, N. Jeffery, and Y. J. Lee (2020), Journal of Geophysical Research: Oceans **125** (9), e2020JC016211.

England, M. R., I. Eisenman, N. J. Lutsko, and T. J. Wagner (2021), Geophysical Research Letters **48** (15), e2021GL094086.

Eppley, R. W. (1972), Fish. bull **70** (4), 1063.

Huisman, J. (1999), Ecology **80** (1), 202.

Köhler, J., L. Wang, A. Guislain, and T. Shatwell (2018), Limnology and Oceanography **63** (3), 1156.

Lester, C. W., T. J. W. Wagner, D. E. McNamara, and M. R. Cape (2021), Geophysical Research Letters **48** (2), e2020GL091758.

Leu, E., C. J. Mundy, P. Assmy, K. Campbell, T. M. Gabrielsen, M. Gosselin, T. Juul-Pedersen, and R. Gradinger (2015), Progress in Oceanography **139**, 151.

Lewis, K., A. Arntsen, P. Coupel, H. Joy-Warren, K. Lowry, A. Matsuoka, M. Mills, G. Van Dijken, V. Selz, and K. Arrigo (2019), Limnology and Oceanography **64** (1), 284.

Lewis, K., G. Van Dijken, and K. R. Arrigo (2020), Science **369** (6500), 198.

Lorenzen, C. J. (1972), ICES Journal of Marine Science **34** (2), 262.

Matrai, P., E. Olson, S. Suttles, V. Hill, L. Codispoti, B. Light, and M. Steele (2013), Progress in Oceanography **110**, 93.

Mayot, N., P. Matrai, A. Arjona, S. Bélanger, C. Marchese, T. Jaegler, M. Ardyna, and M. Steele (2020), Journal of Geophysical Research: Oceans **125** (3), e2019JC015799.

Moreau, S., D. Lannuzel, J. Janssens, M. Arroyo, M. Corkill, E. Cougnon, C. Genovese, B. Legresy, A. Lenton, V. Puigcorbe, *et al.* (2019), Journal of Geophysical Research: Oceans **124** (5), 2943.

NASA Ocean Biology Processing Group, GSFC, (2017), doi:10.5067/NPP/VIIRS/L3M/CHL/2018.

NASA Ocean Biology Processing Group, GSFC, (2021), doi:10.5067/AQUA/MODIS/L3M/CHL/2021.

NASA Ocean Biology Processing Group, GSFC, (2022), doi:10.5067/TERRA/MODIS/L3M/CHL/2022.

Norrbin, F., H. C. Eilertsen, and M. Degerlund (2009), Deep Sea Research Part II: Topical Studies in Oceanography **56** (21-22), 1945.

Nöthig, E.-M., A. Bracher, A. Engel, K. Metfies, B. Niehoff, I. Peeken, E. Bauerfeind, A. Cherkasheva, S. Gäbler-Schwarz, K. Hardge, *et al.* (2015), Polar Research **34** (1), 23349.

Peralta-Ferriz, C., and R. A. Woodgate (2015), Progress in Oceanography **134**, 19.

Richardson, K., S. Markager, E. Buch, M. F. Lassen, and A. S. Kristensen (2005), Deep Sea Research Part I: Oceanographic Research Papers **52** (6), 979.

Smith Jr, W. O., M. E. Baumann, D. L. Wilson, and L. Aletsee (1987), Journal of Geophysical Research: Oceans **92** (C7), 6777.

Smith Jr, W. O., and R. M. Jones (2015), ICES Journal of Marine Science **72** (6), 1952.

Søreide, J. E., E. V. Leu, J. Berge, M. Graeve, and S. Falk-Petersen (2010), Global change biology **16** (11), 3154.

Supply, A., J. Boutin, J.-L. Vergely, N. Kolodziejczyk, G. Reverdin, N. Reul, and A. Tarasenko (2020), Remote Sensing of Environment **249**, 112027.

Talling, J. (1957), The New Phytologist **56** (2), 133.

Wassmann, P., and M. Reigstad (2011), Oceanography **24** (3), 220.

Zhao, H., A. Matsuoka, M. Manizza, and A. Winter (2022), Journal of Geophysical Research: Oceans , e2021JC018346.

Supplementary Information:
A model of near-sea ice phytoplankton blooms

C. W. Lester,[1,*] T. J. W. Wagner,[2] and Dylan E. McNamara[3]

[1] *Earth and Climate Sciences, Duke University*
[2] *Atmospheric and Oceanic Sciences, University of Wisconsin Madison*
[3] *Physics and Physical Oceanography, University of North Carolina Wilmington*

S1. PHYTOPLANKTON DISTRIBUTION IN A MIXED LAYER

We consider the evolution of phytoplankton concentration $p(z, \boldsymbol{x}, t)$ (mass of plankton per unit volume) as a passive tracer, the dynamics of which are governed by

$$\mathrm{D}_t p = \widetilde{\Gamma} p, \tag{S1}$$

where D_t is the material derivative and $\widetilde{\Gamma}$ is the net growth rate which is generally composed of phytoplankton production from light and nutrient uptake and losses from mortality, respiration, sinking, and predation.

Here, we are interested in the evolution of $p(z, \boldsymbol{x}, t)$ as averaged over the surface mixed layer with depth boundary $D(\boldsymbol{x}, t)$. We take the phytoplankton to be well mixed within the surface mixed layer, such that $p(z, \boldsymbol{x}, t) = P(\boldsymbol{x}, t) + p'(z, \boldsymbol{x}, t)$, where $P(\boldsymbol{x}, t)$ is the depth averaged plankton concentration and $p'(z, \boldsymbol{x}, t)$ are considered small perturbations from the average. Similarly, the horizontal flow field is regarded as the depth averaged flow $\boldsymbol{u}(\boldsymbol{x}, t)$ plus fluctuations $\boldsymbol{u}'(z, \boldsymbol{x}, t)$. Averaging over the fast fluctuation time scales and over depth $z = [0, D]$, Equation (S1) reduces to Equation (1).

S2. QUASI-STEADY DYNAMICS

To facilitate direct comparisons to satellite data, we consider the quasi-steady state dynamics of the system (see "An Idealized Model Of Near-Ice Bloom Dynamics" Section in the main text). The phytoplankton evolution averaged along the ice edge and over monthly time scales can then be approximated as

$$U \frac{\mathrm{d}\overline{P}}{\mathrm{d}x} \simeq \Gamma(\overline{P}, \overline{D})\overline{P} + \kappa \frac{\mathrm{d}^2 \overline{P}}{\mathrm{d}x^2}$$

where κ is the turbulent diffusivity. The main effect of κ in this framework is to smooth $\overline{P}(x)$. We can define the Péclet number $\mathrm{Pe} = |\Gamma|^{-1} U^2/\kappa$, where $|\Gamma|^{-1} U$ is the characteristic bloom length scale given by the ratio of the advection scale U and growth rate $|\Gamma|$. Here, κ/U is the characteristic turbulent length scale. For $\mathrm{Pe} \gg 1$ turbulent diffusion

* Corresponding author contact: conner.lester@duke.edu

becomes negligible and the system is governed by mean advection. For a typical growth rate scale $|\Gamma| \sim 0.1$ day^{-1} and $U \sim 0.1$ m/s, the bloom length is of order ~ 100 km (Figure 1). Ocean diffusivity scales are of order 100 m^2/s suggesting turbulent lengths of order kilometers. Thus we assume a regime where Pe $\gg 1$ and are left with the time averaged model in the main text (Equations 4). As in the main text, we omit the overlines for below for clarity: $\overline{P} \to P$, $\overline{D} \to D$.

S3. GROWTH RATE

In main text Section "An Idealized Model Of Near-Ice Bloom Dynamics" we discuss the assumption that phytoplankton growth is mainly determined by sunlight availability. Specifically, we assume that growth rate Γ is dependent on light intensity $\widetilde{I}(p,z) \simeq \widetilde{I}(P,z)$ but not inhibited by nutrient limitations within the mixed layer (noting that we are primarily interested in early spring blooms where nutrients have typically not depleted).

The light intensity (normalized by the surface value) at depth z is given by the Beer-Lambert Law as

$$\widetilde{I}(P,z) = \exp\left(-\frac{z}{\ell_f} - \frac{P}{\rho_P}\frac{z}{\ell_P}\right) \equiv \exp\left(-\frac{z}{\ell_0}\right),$$

with the characteristic decay length defined by $1/\ell_0 \equiv 1/\ell_f + P/K_B$, where ℓ_f is the fluid light attenuation length, $K_B = \rho_P \ell_P$ is an effective biomass carrying capacity scale set by the average single-cell phytoplankton density ρ_P, and the phytoplankton light attenuation length ℓ_P (Huisman 1999). For light dependent phytoplankton growth, controlled experiments show that the growth rate scales linearly with low light intensity (light-limited regime) relative to a respiration threshold, whereas for large light intensities the growth rate becomes roughly constant (saturated regime) (Eilers and Peeters 1988; Hintz *et al.* 2022). Under fluctuating light conditions, as in a mixed layer, the saturated regime occurs at much larger light intensities than in constant light conditions (Köhler *et al.* 2018). For this reason and because the depth averaged light intensity varies relatively slowly, we approximate the phytoplankton growth-light relationship as linear. Thus we write the net depth-averaged growth rate as

$$\Gamma(P,D) \simeq \gamma I(P,D) - r - w_P/D - w(D)/D,$$

as in Equation (2). Here, γ is the growth rate scale proportional to the light intensity at the surface, $I = (\ell_0/D)(1 - e^{-D/\ell_0})$ is the depth-averaged (normalized) light intensity, r is the mortality/respiration rate, and w_P is the phytoplankton sinking velocity.

S4. CONSTRAINTS AND SCALINGS

Equations (1)–(3) present a closed model for near-ice phytoplankton growth and solutions can be obtained once parameters are constrained. Suggested parameter ranges found in the literature are: the light attenuation length

$10 \lesssim \ell_f \lesssim 40$ m (Lorenzen 1972; Sakshaug and Slagstad 1991), the biomass scale $25 \lesssim K_B \lesssim 100$ mg Chl-a/m^2 (Lorenzen 1972; Sosik and Mitchell 1995), the phytoplankton settling rate $0 \lesssim w_P \lesssim 1$ m/day (Chindia and Figueredo 2018; Naselli-Flores *et al.* 2021), the phytoplankton mortality/respiration rate in cold climates $r \lesssim 0.2$ day^{-1} (Baker and Geider 2021), and the average flow velocity normal to the ice edge in Fram Strait $U \lesssim 0.2$ m/s (Beszczynska-Möller *et al.* 2012). We assume the following parameter values in Figure 4: $\ell_f = 20$ m, $K_B = 50$ mg Chl-a/m^2, $w_P = 1$ m/day, $r = 0.1$ day^{-1} and $U = 0.1$ m/s.

The remaining parameters values to constrain are $P_\infty,\ P_0,\ \gamma,\ D_\infty$ and D_0. $P(x \to \infty) = P_\infty$ and $P(x = 0) = P_0$ are inferred from from chl-a observations in Figure 4 (see SI Section S5 below). The growth rate scale γ is in principle given by the surface light intensity. However, predictions of surface light intensity in Fram Strait are often only provided for cloudless skies and the presence of clouds can reduce the light intensity by nearly an order of magnitude (Sakshaug and Slagstad 1991). Here, we choose to extract an effective growth rate γ via the exponential growth length scale L_P (Eq. 5) as defined by

$$\frac{U\gamma^{-1}}{L_P} = I(P_0, D_0) - \frac{r}{\gamma} - \frac{w_P}{\gamma D_0} - \frac{U\gamma^{-1}}{L_P}\left(1 - \frac{D_0}{D_\infty}\right), \tag{S2}$$

where most of the monthly variations in L_P seem to be set by γ (Figure 4). Similarly, information about the open ocean mixed layer depth is (in principle) encapsulated in the dynamics of $P(x)$—specifically in P_∞. Thus D_∞ can be solved for when $\Gamma = 0$ or:

$$I(P_\infty, D_\infty) - \frac{r}{\gamma} - \frac{w_P}{\gamma D_\infty} = 0. \tag{S3}$$

To a good approximation the open ocean phytoplankton concentration is in this case given by

$$P_\infty \simeq \frac{K_B}{D_\infty}\left(\frac{\gamma}{r + \frac{w_P}{D_\infty}} - \frac{D_\infty}{\ell_f}\right), \tag{S4}$$

showing that the open ocean concentration is set by the biomass capacity K_B relative to the open ocean mixed layer depth D_∞. It also increases with light intensity γ. This also suggests that $D_\infty \lesssim \gamma\ell_f/r$, otherwise the open ocean concentration would vanish. We note that this is a recovery of the "critical depth" scaling of Sverdrup (1953). The remaining parameter that remains unconstrained is the depth of the mixed layer at the ice edge D_0, which is used as a fitting parameter selected within observational ranges (Peralta-Ferriz and Woodgate 2015; von Appen *et al.* 2021; Park *et al.* 1999).

The maximum phytoplankton concentration $P_{\max}$ occurs for $\Gamma = 0$ at a characteristic mixed layer depth $D_* = D(P_{\max})$ as

$$P_{\max} \simeq \frac{K_B}{D_*}\left(\frac{\gamma}{r + \frac{w_P}{D_*} + \frac{U}{L_D}\left(1 - \frac{D_*}{D_\infty}\right)} - \frac{D_*}{\ell_f}\right). \tag{S5}$$

Because $P_{\max}$ occurs close to the ice edge, the characteristic depth scales as $D_* \propto D_0$. It is found that the mixed layer depth at the ice edge decreases as the sea ice melt rate M_0 increases, such that $D_0 \sim 1/M_0$ (Castagno *et al.* 2023). Combining this with the approximate relationship $P_{\max} \sim 1/D_0$ suggests the scaling $P_{\max} \sim \gamma K_B M_0$.

We note that the characteristic relationships above (Eq.'s S2-S5) show that the system is governed by 6 dimensionless groupings of the 10 total parameters:

$$\frac{P_\infty}{P_0}, \quad \frac{D_\infty}{D_0}, \quad \frac{L_P}{U\gamma^{-1}}, \quad \frac{r}{\gamma}, \quad \frac{w_P}{\gamma D_0}, \quad \frac{L_D}{U\gamma^{-1}}. \tag{S6}$$

And if we take P_∞/P_0 and $L_P/U\gamma^{-1}$ as well constrained by measurements in Figure 4 (assuming L_P scales with the characteristic growth length $U\gamma^{-1}$), then the model is only sensitive to variations in the remaining 4 parameter groupings.

In Figure S2 we conduct a sensitivity analysis of the model predictions for June measurements of P_0, P_∞ and L_P (Figure 4). The 4 characteristic parameter groupings D_∞/D_0, r/γ, $w_P/\gamma D_0$ and $L_D/U\gamma^{-1}$ are varied within observational ranges while satisfying the constraints of Eq.'s (S2) and (S3). The main variation in model prediction (in the characteristic "bloom curve") is found in the magnitude of the bloom $P_{\max}$ with parameter groupings $L_D/U\gamma^{-1}$ and K_B/P_0D_0 while the peak remains between $1.5L_P$ and $3.5L_P$ or between 100 and 250 km from the ice edge. Since $P_{\max} \sim K_B/D_0$ and also increases with $L_D/U\gamma^{-1}$ (Eq. S5) this variability is reasonable. However, because L_D is a representation of vertical mixing as meltwater is advected from the ice edge, we expect L_D to scale with U (as should L_P).

S5. OBSERVATIONAL DATA

The core observations we use to constrain the model above are satellite measurements of chlorophyll *a* (chl-a), sea surface salinity (SSS), and sea ice concentration (SIC).

Near-surface chl-a concentration data for the years 2011–2019 were averaged over the monthly Level 3 products from three sensors: MODIS Aqua (NASA Ocean Biology Processing Group, GSFC 2021), MODIS Terra (NASA Ocean Biology Processing Group, GSFC 2022), and VIIRS-SPNN (NASA Ocean Biology Processing Group, GSFC 2017), all at 9 km resolution. Note that VIIRS-SPNN only came online in late 2011 and so only covers the spring seasons 2012–2019. We use these datasets rather than the merged Ocean-Colour Climate Change Initiative (OC-CCI) product (Sathyendranath *et al.* 2019) because OC-CCI features large and seemingly spurious variability right at the ice edge (not shown). These issues are not found in the individual sensor data or when computing the average of the three sensors listed above.

To assess the impact of meltwater on surface salinity we use Version 1 of the monthly Level 3 Soil Moisture and Ocean Salinity (SMOS) Arctic SSS product provided by LOCEAN (Supply *et al.* 2020) at 25 km resolution. This product spans from June 2010 to November 2019 and covers the Arctic region north of 60°N. Since we are interested

in the spring bloom period (April–June) we limit our study period to years 2011–2019. To estimate the location of the sea ice edge, we use SIC for Fram Strait spanning the years 2011 to 2019 from SMMR-SSM/I data processed with the NASA Team algorithm (Cavalieri *et al.* 1996) at 25 km resolution.

The focus of this study is how chl-a and SSS vary with distance from the sea ice edge. To compute this dependence, we determine the distance to the sea ice edge (defined as the SIC = 50% contour) for each grid box on all monthly distribution maps. We then calculate the values of chl-a and SSS at each location and bin the data as a function of distance from the ice edge. Finally, we average over the years 2011–2019 to get the decadal-mean monthly curves for April, May, and June as functions of distance from the sea ice edge. The SIC contours for 15%, 50%, and 75% run in approximately straight and parallel lines from the northeast (near Svalbard) to the southwest (see Figure 1). This enables us to consider how chl-a and SSS vary in the direction perpendicular to the ice edge by averaging the data in the direction parallel to the ice edge.

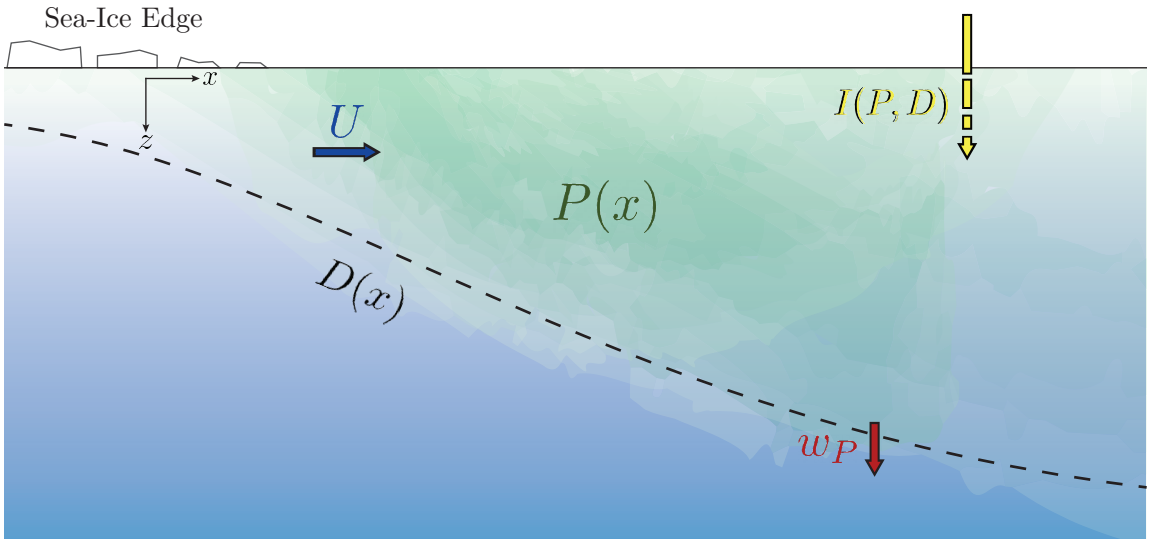

FIG. S1. Schematic of simplified phytoplankton bloom dynamics within a mixed layer stratified by meltwater. Dashed line shows the mixed layer depth $D(x)$ increasing with distance from the ice edge as the sea-ice meltwater mixes increasingly with salty ambient open-ocean waters. The phytoplankton concentration within the mixed layer $P(x)$ is advected from the ice edge at rate U and grows at a rate determined by sunlight intensity averaged over the mixed layer $I(P, D)$. The concentration $P(x)$ decreases from dilution as the mixed layer depth increases $D(x)$, from sinking out of the mixed layer at rate w_P, and from natural mortality/respiration at rate r (not shown).

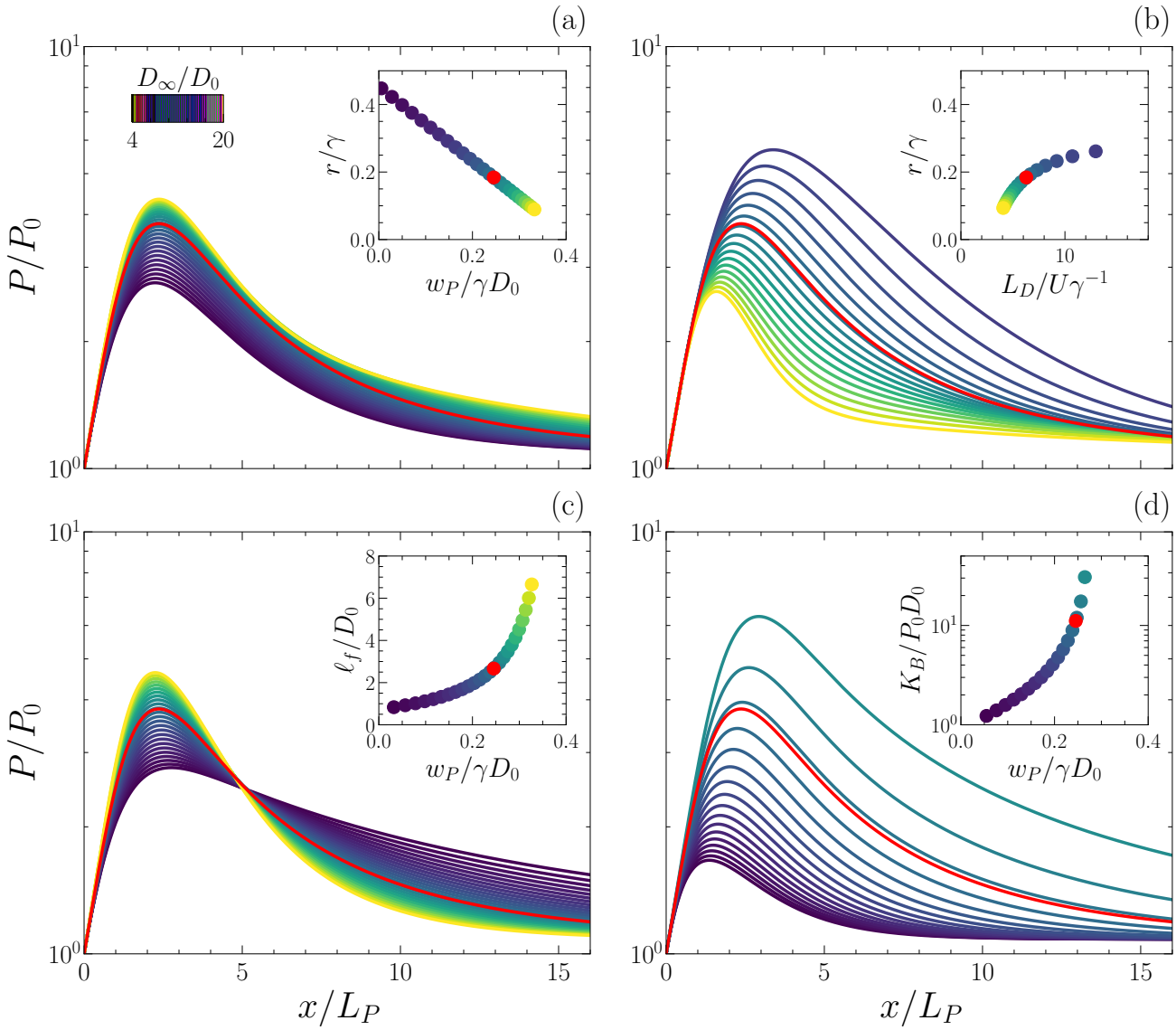

FIG. S2. "Bloom curve" parameter sensitivity. Here we vary model parameters while holding fixed measured chl-a parameters from June, namely the chl-a concentration at the ice edge P_0 and in the open ocean P_∞ and the exponential growth length scale L_P (Figure 4). In all panels (a,b,c,d) we vary the rescaled mixed layer parameter D_∞/D_0 and solve constraint equations (S2) and (S3) for various parameter groupings (insets) while holding the other parameters fixed. Red lines and markers in the insets show values for June used in Figure 4. D_∞/D_0 is varied between $(4, 20)$ broadly approximated for variations in both open ocean and near ice mixed layer depths (Peralta-Ferriz and Woodgate 2015; Park *et al.* 1999). The death/respiration rate rescaled by the growth rate r/γ shows solutions for values $\lesssim 0.5$ for June parameters (insets a,b). Although r represents uncertain and complex processes, $r/\gamma \lesssim 0.5$ is reasonable for respiration and growth rate ranges in cold water growth conditions (as natural cell death is slowed at low temperatures) (Baker and Geider 2021; Eppley 1972; Smith Jr *et al.* 1987). The phytoplankton settling rate w_P tends to be $\lesssim 1$ m/d or so depending on the size and type of phytoplankton (Chindia and Figueredo 2018; Naselli-Flores *et al.* 2021). Thus we expect the settling length $w_P/\gamma \lesssim 2$ m, and so $w_P/\gamma D_0 \lesssim 0.5$ (insets a,c,d) for $D_0 \gtrsim 5$ m (Peralta-Ferriz and Woodgate 2015; Park *et al.* 1999). Average surface velocities normal to the ice edge U in Fram Straight vary roughly around 10 km/d (Beszczynska-Möller *et al.* 2012). The inset ranges in panel (b) are for the length $U/\gamma \sim (10, 20)$ km and assuming a broad range of $L_D \sim (50, 150)$ km—we note however that the vertical mixing length L_D likely scales with U. The light attenuation length ℓ_f for clear water varies between around 10 and 40 meters or so (Lorenzen 1972; Sakshaug and Slagstad 1991) thus we vary $\ell_f/D_0 \lesssim 8$ in panel (c). The biomass scale varies broadly around averages of $K_B \sim (25, 100)$ mg Chl-a/m^2 set by light absorption properties of Chl-a (Lorenzen 1972; Sosik and Mitchell 1995). Thus we allow a broad range of $K_B/P_0D_0 \sim (1, 50)$ in panel (d).

J. Huisman, Population dynamics of light-limited phytoplankton: microcosm experiments, Ecology **80**, 202 (1999).

P. Eilers and J. Peeters, A model for the relationship between light intensity and the rate of photosynthesis in phytoplankton, Ecological modelling **42**, 199 (1988).

N. H. Hintz, B. Schulze, A. Wacker, and M. Striebel, Ecological impacts of photosynthetic light harvesting in changing aquatic environments: A systematic literature map, Ecology and Evolution **12**, e8753 (2022).

J. Köhler, L. Wang, A. Guislain, and T. Shatwell, Influence of vertical mixing on light-dependency of phytoplankton growth, Limnology and Oceanography **63**, 1156 (2018).

C. J. Lorenzen, Extinction of light in the ocean by phytoplankton, ICES Journal of Marine Science **34**, 262 (1972).

E. Sakshaug and D. Slagstad, Light and productivity of phytoplankton in polar marine ecosystems: a physiological view, Polar Research **10**, 69 (1991).

H. M. Sosik and B. G. Mitchell, Light absorption by phytoplankton, photosynthetic pigments and detritus in the california current system, Deep Sea Research Part I: Oceanographic Research Papers **42**, 1717 (1995).

J. A. Chindia and C. C. Figueredo, Phytoplankton settling depends on cell morphological traits, but what is the best predictor?, Hydrobiologia **813**, 51 (2018).

L. Naselli-Flores, T. Zohary, and J. Padisák, Life in suspension and its impact on phytoplankton morphology: an homage to colin s. reynolds, Hydrobiologia **848**, 7 (2021).

K. G. Baker and R. J. Geider, Phytoplankton mortality in a changing thermal seascape, Global Change Biology **27**, 5253 (2021).

A. Beszczynska-Möller, E. Fahrbach, U. Schauer, and E. Hansen, Variability in atlantic water temperature and transport at the entrance to the arctic ocean, 1997–2010, ICES Journal of Marine Science **69**, 852 (2012).

H. Sverdrup, On conditions for the vernal blooming of phytoplankton, J. Cons. Int. Explor. Mer **18**, 287 (1953).

C. Peralta-Ferriz and R. A. Woodgate, Seasonal and interannual variability of pan-arctic surface mixed layer properties from 1979 to 2012 from hydrographic data, and the dominance of stratification for multiyear mixed layer depth shoaling, Progress in Oceanography **134**, 19 (2015).

W.-J. von Appen, A. M. Waite, M. Bergmann, C. Bienhold, O. Boebel, A. Bracher, B. Cisewski, J. Hagemann, M. Hoppema, M. H. Iversen, *et al.*, Sea-ice derived meltwater stratification slows the biological carbon pump: results from continuous observations, Nature Communications **12**, 7309 (2021).

M. G. Park, S. R. Yang, S.-H. Kang, K. H. Chung, and J. H. Shim, Phytoplankton biomass and primary production in the marginal ice zone of the northwestern weddell sea during austral summer, Polar Biology **21**, 251 (1999).

A. P. Castagno, T. J. W. Wagner, M. R. Cape, C. W. Lester, E. Bailey, C. Alves-de Souza, R. A. York, and A. H. Fleming, Increased sea ice melt as a driver of enhanced arctic phytoplankton blooming, Global Change Biology **29**, 5087 (2023), https://onlinelibrary.wiley.com/doi/pdf/10.1111/gcb.16815.

NASA Ocean Biology Processing Group, GSFC, Moderate-resolution Imaging Spectroradiometer (MODIS) Aqua Level-3 Standard Mapped Image CHL Data doi:10.5067/AQUA/MODIS/L3M/CHL/2021 (2021).

NASA Ocean Biology Processing Group, GSFC, Terra MODIS Level 3 Mapped Chlorophyll Data, Version R2022.0 doi:10.5067/TERRA/MODIS/L3M/CHL/2022 (2022).

NASA Ocean Biology Processing Group, GSFC, VIIRS-SNPP Level 3 Mapped Chlorophyll Data Version R2018.0 doi:10.5067/NPP/VIIRS/L3M/CHL/2018 (2017).

S. Sathyendranath, R. J. Brewin, C. Brockmann, V. Brotas, B. Calton, A. Chuprin, P. Cipollini, A. B. Couto, J. Dingle, R. Doerffer, *et al.*, An ocean-colour time series for use in climate studies: the experience of the ocean-colour climate change initiative (OC-CCI), Sensors **19**, 4285 (2019).

A. Supply, J. Boutin, J.-L. Vergely, N. Kolodziejczyk, G. Reverdin, N. Reul, and A. Tarasenko, New insights into smos sea surface salinity retrievals in the arctic ocean, Remote Sensing of Environment **249**, 112027 (2020).

D. J. Cavalieri, C. Parkinson, P. Gloersen, and H. J. Zwally, Sea ice concentrations from Nimbus-7 SMMR and DMSP SSM/I-SSMIS passive microwave data (1996).

R. W. Eppley, Temperature and phytoplankton growth in the sea, Fish. bull **70**, 1063 (1972).

W. O. Smith Jr, M. E. Baumann, D. L. Wilson, and L. Aletsee, Phytoplankton biomass and productivity in the marginal ice zone of the fram strait during summer 1984, Journal of Geophysical Research: Oceans **92**, 6777 (1987).